Applied Physics Letters

RESEARCH ARTICLE | SEPTEMBER 23 2025

Boosting the electrocaloric effect with broad working temperature span in lead-free relaxor ferroelectrics through disorder modulation

Zixuan Wu ; Wanting Hu ; Krishnarjun Banerjee ; Vladimir Koval ; Haixue Yan ; Man Zhang

Appl. Phys. Lett. 127, 122903 (2025)
https://doi.org/10.1063/5.0289139

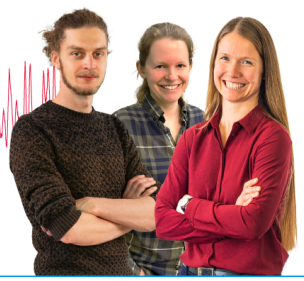

Applied Physics Letters ARTICLE pubs.aip.org/aip/apl

Boosting the electrocaloric effect with broad working temperature span in lead-free relaxor ferroelectrics through disorder modulation

Cite as: Appl. Phys. Lett. **127**, 122903 (2025); doi: 10.1063/5.0289139
Submitted: 5 July 2025 · Accepted: 1 September 2025 ·
Published Online: 23 September 2025

Zixuan Wu,[1] Wanting Hu,[1] Krishnarjun Banerjee,[1] Vladimir Koval,[2] Haixue Yan,[1] and Man Zhang[3,a)]

AFFILIATIONS

[1]School of Engineering and Materials Science, Queen Mary University of London, Mile End Road, London E1 4NS, United Kingdom
[2]Institute of Materials Research, Slovak Academy of Sciences, Watsonova 47, Kosice 040 01, Slovakia
[3]School of Mechanical Engineering, University of Leeds, Woodhouse, Leeds LS2 9JT, United Kingdom

[a)]Author to whom correspondence should be addressed: M.Zhang7@leeds.ac.uk

ABSTRACT

Achieving both high electrocaloric effect and broad working temperature span in ferroelectric materials is crucial for practical cooling applications, yet it remains a big challenge. In the present work, a large electrocaloric temperature change (ΔT) over a wide temperature range is obtained through disorder modulation of perovskite titanates, specifically by introducing an electric field-sensitive $Bi_{0.5}Na_{0.5}TiO_3$ (BNT) into $Ba_{0.6}Sr_{0.4}TiO_3$ (BST). Ceramic samples in the BST-100xBNT ($0.2 \leq x \leq 0.28$) solid solution system show typical characteristics of relaxor ferroelectrics with a high density of polar nano-regions due to short-range ordering of A-site cations. As the concentration of BNT (x) increases, the freezing temperature (T_f) decreases and the Burns temperature (T_B) increases, suggesting the extension of the temperature range of the relaxor in the ergodic state. Moreover, the field-induced polarization was found to increase along with x. The observed structurally induced changes in the relaxor behavior are proposed to contribute to the optimal electrocaloric performance of the BST-28BNT ceramic, with a maximum ΔT of 0.91 °C and a maximum working temperature span of 24.4 °C under an applied electric field of 5 kV/mm. The concept of the A-site disorder modulation provides an innovative strategy to develop high-performance electrocaloric materials from lead-free relaxor ceramics.

Exploring the electrocaloric effect (ECE) in solid-state refrigeration is of great significance, as it presents a promising solution to the growing demand of cooling with high energy efficiency and minimal environmental impact.[1–3] The ECE is defined by a reversible temperature change (ΔT), which results from the change of polarization (ΔP) upon the application and/or removal of an electric field in adiabatic systems.[4] Among various electrocaloric active materials, ferroelectrics demonstrate the most pronounced ECE due to their large change of polarization under electric field (dP/dE).[5] However, practical applications of ferroelectrics are limited by technical circumstances.

The first major drawback of classical ferroelectrics involves a relatively low intrinsic ECE (small ΔT). A big ΔT can be, however, achieved by the massive electric field-induced polarization change.[4] In displacive ferroelectrics, the largest dP/dE often occurs just above their Curie point (T_c), where an applied electric field can induce a large polarization change.[6,7] While the T_c of most displacive ferroelectrics is well above room temperature, an electrocaloric device for practical refrigeration applications is expected to operate near or below room temperature. This variance makes a requirement for lowering the T_c down to room temperature. However, according to the AKJ relationship,[8] decreasing the T_c generally leads to a reduction in polarization, which in turn diminishes ΔP and subsequently ΔT. One possible strategy to overcome this limitation is to incorporate a ferroelectric material, which is responsive to an electric field, such as $Bi_{0.5}Na_{0.5}TiO_3$ (BNT), into a low T_c ferroelectric, thus creating a solid-solution ferroelectric system. Such a chemistry-based approach can potentially enhance electric field-induced polarization change, thereby increasing the ECE in the ferroelectric material through electric field-induced transitions.[9,10]

Another limitation of using classical displacive ferroelectrics in electrocaloric applications is their narrow temperature range of the maximum ECE, limiting the working temperature of cooling devices.

The narrow working temperature span is related to the dielectric behavior near T_c, where the dependence of permittivity on temperature shows a sharp peak.[5] An effective way to overcome this shortcoming is to make the dielectric peak broader. The earlier studies on relaxor ferroelectrics have shown that the increase in chemical disorder can significantly increase the temperature range of the permittivity peak due to a higher degree of diffuseness in the phase transition.[11–14] In this context, one can anticipate that the increased A-site disorder in the ferroelectric system consisting of BNT and low T_c perovskite would extend the usable temperature span of the relaxor ceramics for effective electrocaloric cooling.

In this work, $Ba_{0.6}Sr_{0.4}TiO_3$ (BST) is selected as the base material due to its low T_c (~8 °C) and high polarization sensitivity.[15,16] However, BST exhibits low maximum polarization at and above room temperature (<0.1 C/m^2 at 5 kV/mm), resulting in low ECE.[17] To increase the maximum polarization, the electric field-sensitive BNT is introduced into BST. Additionally, as both BNT and BST share the same B-site cation, increasing the amount of BNT is expected to increase the A-site chemical disorder and configurational entropy in the BST-100xBNT solid solution. These structural changes would increase the diffuseness of the ferroelectric phase transition, thereby broadening the working temperature span.

Ceramic samples in the $(1-x)Ba_{0.6}Sr_{0.4}TiO_3$-$xBi_{0.5}Na_{0.5}TiO_3$ system, with x = 0.20, 0.25, and 0.28 (abbreviated as BST-100xBNT), were prepared using the solid-state reaction method. The starting materials were $BaCO_3$ (Alfa Aesar, purity ≥99.8%), $SrCO_3$ (Sigma-Aldrich, ≥99.9%), Bi_2O_3 (Sigma-Aldrich, ≥99.9%), Na_2CO_3 (Sigma-Aldrich, ≥99.5%), and TiO_2 (Sigma-Aldrich, ≥99.8%). They were dried at 200 °C for 15 h to remove moisture. A stoichiometric amount of raw powders was weighed and then mixed using planetary ball milling (Fritsch Pulverisette 5). The slurry was dried in an oven overnight. The dried powder was calcined at 900 °C for 4 h in a conventional box furnace. To obtain uniform and fine particles, the calcined powder was ball milled again for 4 h. After adding 5 wt. % polyvinyl alcohol at the final stage of the second-round ball milling, the mixture was dried and pressed into pellets under a uniaxial pressure of 200 MPa. The pellets were annealed at 650 °C for 2 h to remove PVA. The green compacts were sintered at 1250 °C for 4 h in a closed alumina crucible with sacrificial powder. To suppress volatilization of Bi and Na, a slow heating rate of 3 °C/min was used during both calcination and sintering, allowing early reaction of the raw materials and enhancing compositional stability.[18]

The density of the samples was measured using Archimedes' principle. The crystal structure of the samples was investigated by x-ray diffraction (XRD, Xpert-Pro) at room temperature. To evaluate phase compositions, the XRD data were analyzed by the Rietveld method using a GSAS-II software package.[19] A scanning electron microscope (SEM, FEI Inspect F) equipped with an energy dispersive x-ray spectrometer (EDS, Oxford Instruments) was used for microstructure observations and elemental mapping in grains and grain boundaries. Differential scanning calorimetry (DSC, DSC 25, TA Instruments) was employed to measure heat capacity (C_p) of the ceramics in a temperature range from 0 to 100 °C at a heating rate of 2 °C/min. For electrical measurements, the disk samples were painted on major surfaces with Ag paste (C2050926P2, SunChemical Ltd.) and then annealed at 650 °C (a firing temperature of Ag paste) for 10 min to obtain the measuring electrodes. The temperature dependencies of the relative dielectric permittivity and loss tangent were measured using an LCR meter (model 4284A, Agilent) at various frequencies from 100 Hz to 100 kHz. The ferroelectric hysteresis loops were measured at various temperatures in silicone oil with a ferroelectric tester (NPL, UK) operated at a frequency of 10 Hz.[20]

The relative density of all the ceramic samples was found to be higher than 95%, indicating good sintering quality. The representative images of microstructures of highly dense BST-100xBNT ceramics are shown in Figs. S1–S3. SEM-EDS analysis confirmed a homogeneous elemental distribution in structural grains of the ceramics under consideration.

Figure 1 displays the refined XRD patterns of the BST-100xBNT ceramics. Apparently, all the samples at room temperature exhibit a mixed-phase structure consisting of tetragonal (space group: *P4mm*) and cubic (space group: *Pm*-3*m*) phases.[21,22] No traces of an impurity phase can be observed in the diffractograms, which indicates that BST and BNT are highly soluble in the BST-100xBNT system. The high solubility makes the formation of A-site disordered perovskite structures possible. The calculated fractions of tetragonal and cubic phases are presented together with the refined lattice parameters in Table SI. From the table, one can see that the fraction of the polar tetragonal phase increases as the amount of the added BNT increases.

Figure 2 shows the temperature dependencies of the relative dielectric permittivity and loss of the BST-100xBNT ceramics. Even though broad and frequency-dependent dielectric permittivity and loss peaks are observed for all the samples, their relaxor behavior around the temperature corresponding to the maximum permittivity (T_m) features significant differences. As can be seen in Fig. 2(a), the BST-20BNT ceramic shows a sharp loss peak, suggesting the contribution from the enhanced movement of ferroelectric domain walls near the ferroelectric phase transition. In contrast, the dielectric response of the BST-25BNT and BST-28BNT samples in Figs. 2(b) and 2(c) is typical of a canonical relaxor with a broad and strong frequency-dependent permittivity vs temperature peak. For better understanding the observed relaxor behavior, the evolution of the Burns temperature (T_B) regarding of the transformation from paraelectric phase to ergodic state and the freezing temperature (T_f), where the material transforms from ergodic state to non-ergodic relaxor, was investigated in relation to the BNT content. The values of T_B and T_f were obtained by extrapolation of the respective Curie–Weiss (C–W) and Vogel–Fulcher (V–F) fitting curves,[23,24] as shown in Fig. S4. Details on the V–F and C–W laws are given in the supplementary material, Eqs. (1) and (2), respectively. The obtained temperatures T_m, T_f, and T_B for the different compositions are summarized in Table I. It is clear that with increasing BNT content, T_f decreases, while the T_m and T_B temperatures increase. This BNT-controlled phase transition behavior leads to a wider temperature range for the ergodic state, where polar nano-regions (PNRs) are electrically active. The temperature stabilization of the ergodic state is an intriguing feature of the BST-100xBNT ceramics because pure BNT has $T_f \sim 190$ °C and $T_m \sim 325$ °C,[9] and the T_c of $Ba_{0.6}Sr_{0.4}TiO_3$ is about 8 °C.[15,16] It should be noted that with increasing x, both T_m and T_B increase. The decrease in T_f can be attributed to the higher degree of the A-site disorder in the relaxor system with the higher BNT content. The random occupation of the A sites by different cations can effectively disrupt long-range ferroelectric ordering in microscopic-sized domains through increased chemical disorder, leading to the increased concentration of PNRs. The higher density of

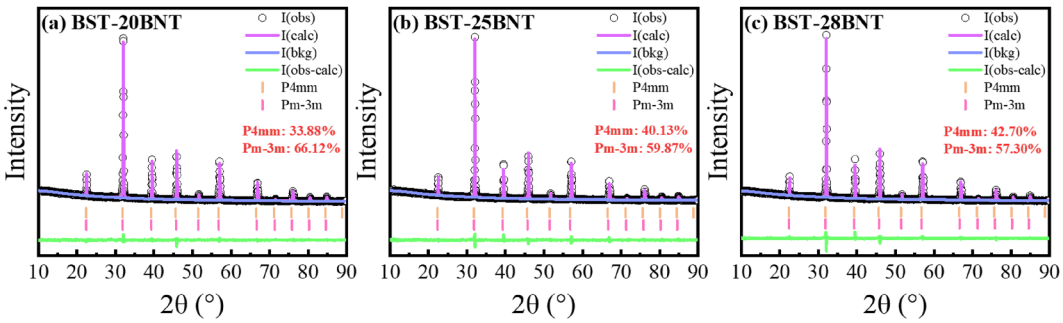

FIG. 1. The refined room temperature XRD patterns of (a) BST-20BNT, (b) BST-25BNT, and (c) BST-28BNT.

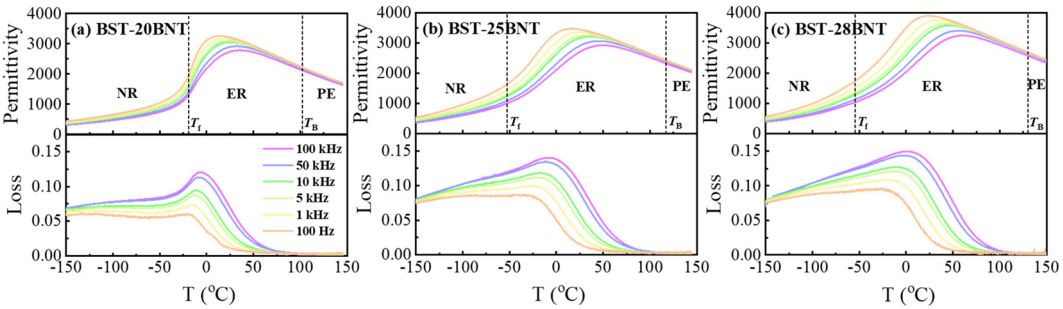

FIG. 2. Temperature dependencies of the relative dielectric permittivity and loss tangent of (a) BST-20BNT, (b) BST-25BNT, and (c) BST-28BNT ceramics (NR: non-ergodic relaxor; ER: ergodic relaxor; PE: paraelectric).

PNRs in the BST-100xBNT ceramics with x = 0.25 and 0.28 results in the pronounced relaxor behavior, as demonstrated in Table I by non-zero and progressively increasing values of ΔT_m. In addition, PNRs are smaller and more active under an applied electric field.

The relaxor behavior of the BST-100xBNT ceramics was investigated by using the modified C–W law [details can be found in the supplementary material, Eq. (3)], where diffuseness coefficient γ was extracted, and it is 2 for ideal diffuse phase transition,[23,25] and the frequency dependence of T_m ($\Delta T_m = T_{m\,100\text{Hz}} - T_{m\,100\,\text{kHz}}$) was also obtained to describe the strength of relaxation behavior.[26] The estimated values of the critical temperature (ΔT_m) and diffuseness coefficient (γ) for the three different compositions are given in Table I. Obviously, with increasing BNT content, both γ and ΔT_m increase, indicating the enhanced degree of the phase transition diffuseness and pronounced relaxor behavior.

Figure 3 shows the polarization–electric field (*P*–*E*) hysteresis loops and current–electric field (*I*–*E*) curves of the BST-100xBNT ceramics, as recorded at different temperatures from 20 to 80 °C. Within the selected temperature range, all the samples exhibit slim *P*–*E* loops, which is a typical feature of relaxor ferroelectrics in ergodic state.[27] The maximum polarization (measured at the same conditions, temperature, and electric field) increases with x, which is beneficial for achieving high ECE. The higher maximum polarization is related to the increased BNT content and high concentration of PNRs, which significantly contribute to the polarization when an external electric field is applied.[28] A broad peak located near zero field in the *I*–*E* plots in Figs. 3(d)–3(f) indicates that all the field-induced transitions in the BST-100xBNT ceramics are mainly reversible.[29]

The ECE in the BST-100xBNT ceramics subjected to the electric field was evaluated by the indirect method based on the Maxwell relation. In this approach, the polarization obtained from the temperature-dependence of the *P*–*E* hysteresis loops is investigated for changes induced by variations in temperature during a certain interval of the applied electric fields. For relaxor ferroelectrics, the indirect method has been demonstrated to provide comparable good results as the direct ECE method, particularly at temperatures well above T_f (i.e.,

TABLE I. The characteristic temperatures and diffuseness coefficient (γ) of the BST-100xBNT ceramics.

Composition	T_f, °C	T_m, °C (1 kHz)	T_B, °C (1 kHz)	ΔT_m, °C (100 Hz–100 kHz)	γ (100 kHz)
BST-20BNT	−19.5	18.3	101.9	22.0	1.58
BST-25BNT	−52.5	24.0	117.5	33.0	1.60
BST-28BNT	−54.7	34.2	130.5	36.2	1.63

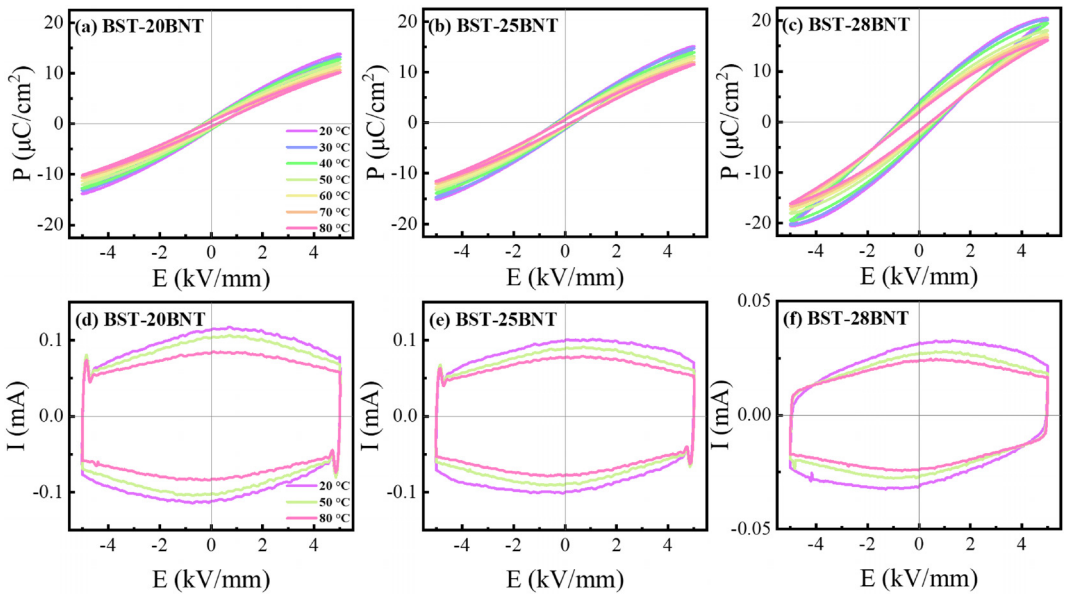

FIG. 3. *P–E* (a)–(c) and corresponding *I–E* (d)–(f) loops of the respective BST-20BNT, BST-25BNT, and BST-28BNT ceramics, as collected at different temperatures (from 20 to 80 °C) under an electric field of 5 kV/mm.

in ergodic state of a relaxor). This is especially true under conditions where there are no abrupt ergodic to non-ergodic transitions and the electric field is relatively low.[30,31]

To evaluate the ECE in the ceramics under consideration, the electrocaloric temperature change (ΔT) was calculated from the following equation:[4]

$$\Delta T = \int_{E_1}^{E_2} -\frac{T}{\rho C_p}\left(\frac{\partial P}{\partial T}\right)_E dE, \quad (1)$$

where ρ is the mass density (determined by the Archimedes method), and C_p is the specific heat capacity of the sample (determined from DSC measurements). E_1 and E_2 are the initial and final electric fields, respectively.

Figure 4(a) shows the maximum polarization as a function of temperature. From the figure, one can see that the polarization of all three materials decreases with increasing temperature. Similarly, as shown in Fig. 4(b), C_p of the ceramics increases on heating. Also, the dependence of the calculated ΔT (at 5 kV/mm) on temperature in Fig. 4(c) features similar trends as the temperature dependence of the relative dielectric permittivity, an initial increase followed by a gradual decrease as the temperature rises. For all three compositions, the highest ΔT occurs at temperatures just above T_m. This finding is consistent with the results of our previous work.[32] The variation of ΔT with temperature depends on the evolution of PNRs, reflecting the competing effect of the decreasing polarization and increasing thermal instability of PNRs with increasing temperature.

Comparing the ECE of all the samples, it is found that the maximum ΔT (ΔT_{max}) increases with the BNT content, reaching the highest value $\Delta T_{max} = 0.91$ °C under an applied electric field of 5 kV/mm in the BST-28BNT sample. It is worth noting that higher ΔT values have been reported in very thin ceramic samples under relatively high electric fields. However, the reduced thickness brings about the risk of undesirable dielectric breakdown.[33] In the present work, the disk-shaped ceramic samples have a thickness of about 0.5 mm, and they were tested under relatively low electric fields to ensure sufficient material volume for effective cooling. The increased ΔT of the x = 0.28 sample is attributed to the higher polarization change substantially contributed by dynamic PNRs. In this study, the temperature span (T_{span}) was calculated as the temperature range where $\Delta T \geq 0.8\Delta T_{max}$,[34,35] as shown in Fig. 4(c). With increasing BNT content, T_{span} becomes broader, indicating an extended effective working temperature range for electrocaloric applications. The highest T_{span} of 24.4 °C under an applied electric field of 5 kV/mm was found in the BST-28BNT sample and can be linked with (i) the wide gap between the T_f and T_B temperatures and (ii) the enhanced diffuseness of the ferroelectric transition caused by the promoted A-site cation disorder. As shown in Fig. S5, the increase in entropy with rising BNT content, driven by enhanced A-site disorder, promotes the formation of PNRs by inducing a local stress field and heterogeneous charge distribution,[36] thereby contributing to enhanced electrocaloric performance. The electrocaloric effect of the BST-28BNT ceramic is comparable with that reported for typical lead-free bulk ceramics derived from $BaTiO_3$,[37,38] $Bi_{0.5}Na_{0.5}TiO_3$,[10,39] $NaNbO_3$,[40] and $K_{0.5}Na_{0.5}NbO_3$.[41] Figures 4(d)–4(f) show the temperature dependencies of the pyroelectric coefficient $-(dP/dT)_E$ of the BST-100xBNT ceramics subjected to an electric field of 1–5 kV/mm. By comparing the pyroelectric behavior of the samples, it is clear that the BST-28BNT ceramic exhibits the strongest polarization sensitivity, yielding the widest temperature span of electrocaloric cooling.

In conclusion, BST-100xBNT (x = 0.20, 0.25, and 0.28) ceramics were fabricated through solid-state reaction. The introduction of BNT into BST resulted in enhanced field-induced polarization and its high sensitivity. For the BST-28BNT ceramic, the large electrocaloric temperature change ΔT of 0.91 °C and wide temperature span T_{span} of

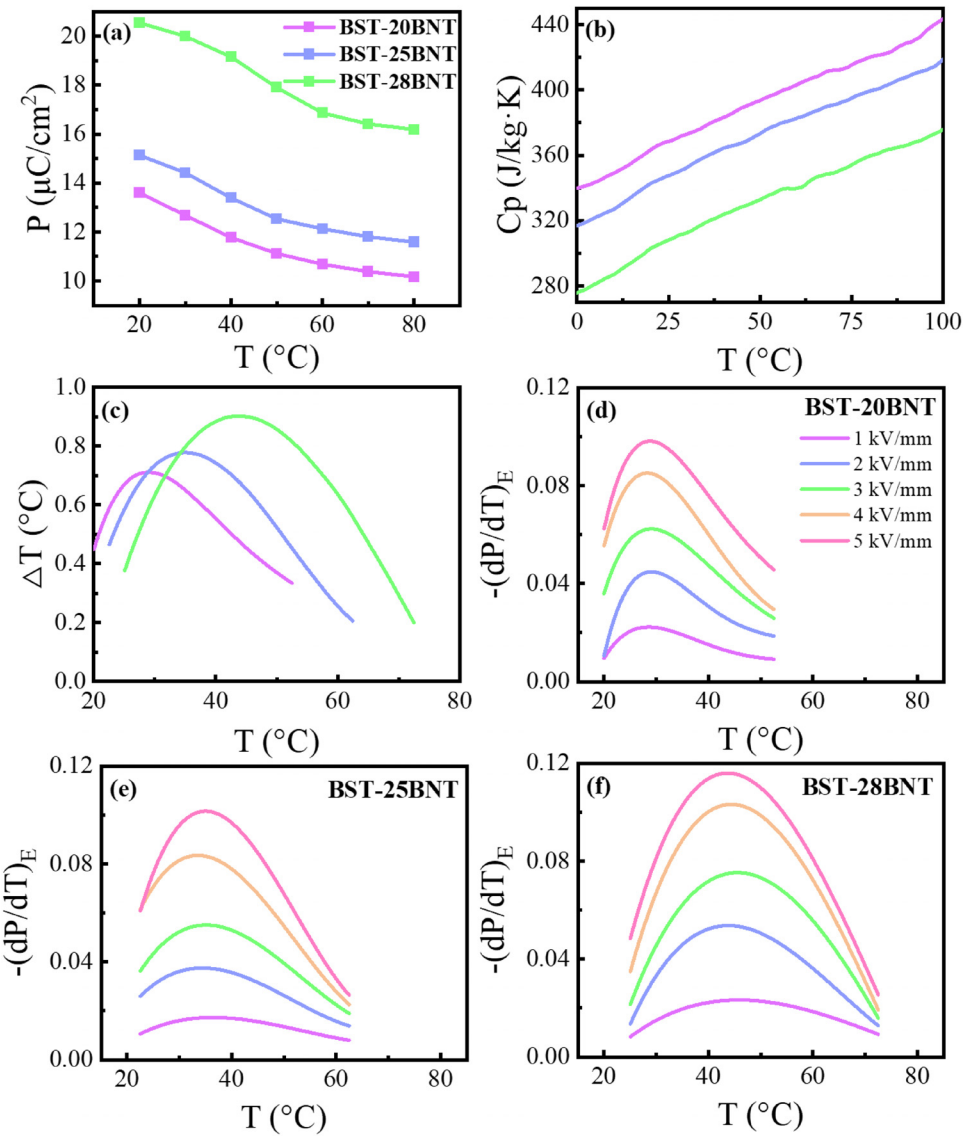

FIG. 4. Temperature dependencies of (a) polarization, (b) heat capacity, (c) electrocaloric temperature change under an electric field of 5 kV/mm for the BST-100xBNT ceramics [in (a), the solid squares represent data extracted from Figs. 3(a)–3(c), the solid lines are fitted data]. (d)–(f) Temperature dependencies of the pyroelectric coefficient of the BST-100xBNT ceramics under an electric field of 1–5 kV/mm.

24.4 °C under an applied electric field of 5 kV/mm were obtained and attributed to the extended temperature gap between T_f and T_B and increased degree of diffuseness in the ferroelectric phase transition. The proposed approach of the A-site disorder modulation provides a viable way for achieving a high ECE over a wide temperature range in lead-free relaxor ceramics.

See the supplementary material for the SEM images, EDS maps, refined XRD data and parameters, detailed descriptions of the V–F and C–W laws, selected and fitted dielectric data, and composition-dependent A-site configurational entropy of BST-100BNT ceramics.

Z.W. and W.H. acknowledge the financial support from the China Scholarship Council (CSC) under Grant Nos. 202207000015 and 202106370015. K.B. acknowledges the financial support from the Engineering and Physical Sciences Research Council (Grant No. EP/Y027752/1). V.K. acknowledges the financial support from the Grant Agency of the Slovak Academy of Sciences (VEGA No. 2/0034/23). M.Z. acknowledges the finical support from the Royal Society of Chemistry (No. R24-1199482977).

AUTHOR DECLARATIONS

Conflict of Interest

The authors have no conflicts to disclose.

Author Contributions

Zixuan Wu: Conceptualization (equal); Data curation (equal); Formal analysis (equal); Investigation (equal); Validation (equal); Visualization (equal); Writing – original draft (equal); Writing – review & editing (equal). **Wanting Hu:** Formal analysis (equal); Methodology (equal); Writing – review & editing (equal). **Krishnarjun Banerjee:** Formal analysis (equal); Methodology (equal); Writing – review & editing (equal). **Vladimir Koval:** Formal analysis (equal); Methodology (equal); Writing – review & editing (equal). **Haixue Yan:** Conceptualization (equal); Funding acquisition (equal); Supervision (equal); Writing – review & editing (equal). **Man Zhang:** Conceptualization (equal); Funding acquisition (equal); Supervision (equal); Writing – review & editing (equal).

DATA AVAILABILITY

The data that support the findings of this study are available from the corresponding author upon reasonable request.

REFERENCES

[1]J. F. Scott, Annu. Rev. Mater. Res. **41**(1), 229 (2011).
[2]M. Valant, Prog. Mater. Sci. **57**(6), 980 (2012).
[3]J. Shi, D. Han, Z. Li, L. Yang, S.-G. Lu, Z. Zhong, J. Chen, Q. M. Zhang, and X. Qian, Joule **3**(5), 1200 (2019).
[4]G. G. Wiseman, IEEE Trans. Electron Devices **16**(6), 588 (1969).
[5]M. C. Rose and R. E. Cohen, Phys. Rev. Lett. **109**(18), 187604 (2012).
[6]G. Shirane and S. Hoshino, J. Phys. Soc. Jpn. **6**, 265 (1951).
[7]M. Harwood, P. Popper, and D. Rushman, Nature **160**, 58 (1947).
[8]S. C. Abrahams, S. K. Kurtz, and P. B. Jamieson, Phys. Rev. **172**(2), 551 (1968).
[9]B. N. Rao, R. Datta, S. S. Chandrashekaran, D. K. Mishra, V. Sathe, A. Senyshyn, and R. Ranjan, Phys. Rev. B **88**(22), 224103 (2013).
[10]F. Li, X. Wang, M. Long, D. Q. Tan, L. Shan, C. Wang, and H. Yan, Acta Mater. **293**, 121093 (2025).
[11]G. A. Samara, J. Phys.: Condens. Matter **15**, 367 (2003).
[12]A. A. Bokov and Z. G. Ye, J. Mater. Sci. **41**(1), 31 (2006).
[13]A. S. Mischenko, Q. Zhang, R. W. Whatmore, J. F. Scott, and N. D. Mathur, Appl. Phys. Lett. **89**(24), 242912 (2006).
[14]W. Liu, F. Li, G. Chen, G. Li, J. Zhai, M. Long, C. Wang, and L. Shan, Scr. Mater. **215**, 114713 (2022).
[15]L. Zhou, P. M. Vilarinho, and J. L. Baptista, J. Eur. Ceram. Soc. **19**(11), 2015 (1999).
[16]V. V. Lemanov, E. P. Smirnova, P. P. Syrnikov, and E. A. Tarakanov, Phys. Rev. B **54**(5), 3151 (1996).
[17]H. Zhang, H. Giddens, Y. Yue, X. Xu, V. Araullo-Peters, V. Koval, M. Palma, I. Abrahams, H. Yan, and Y. Hao, J. Eur. Ceram. Soc. **40**(12), 3996 (2020).
[18]M. Li, M. J. Pietrowski, R. A. De Souza, H. Zhang, I. M. Reaney, S. N. Cook, J. A. Kilner, and D. C. Sinclair, Nat. Mater. **13**(1), 31 (2014).
[19]B. H. Toby and R. B. Von Dreele, J. Appl. Crystallogr. **46**(2), 544 (2013).
[20]M. Zhang, X. Xu, S. Ahmed, Y. Yue, M. Palma, P. Svec, F. Gao, I. Abrahams, M. J. Reece, and H. Yan, Acta Mater. **229**, 117815 (2022).
[21]R. S. Liu, Y. C. Cheng, J. M. Chen, R. G. Liu, J. L. Wang, J. C. Tsai, and M. Y. Hsu, Mater. Lett. **37**(4-5), 285 (1998).
[22]S. Maity, A. Sasmal, and S. Sen, J. Alloys Compd. **884**, 161072 (2021).
[23]H. Zhang, B. Yang, A. D. Fortes, H. Yan, and I. Abrahams, J. Mater. Chem. A **8**(45), 23965 (2020).
[24]K. B. Lyons, P. A. Fleury, and D. Rytz, Phys. Rev. Lett. **57**(17), 2207 (1986).
[25]K. Uchino and S. Nomura, Ferroelectrics **44**(1), 55 (1982).
[26]Y. Yue, X. Xu, M. Zhang, Z. Yan, V. Koval, R. M. Whiteley, D. Zhang, M. Palma, I. Abrahams, and H. Yan, ACS Appl. Mater. Interfaces **13**(48), 57548 (2021).
[27]L. Jin, F. Li, S. Zhang, and D. J. Green, J. Am. Ceram. Soc. **97**(1), 1 (2014).
[28]D. Fu, H. Taniguchi, M. Itoh, S. Y. Koshihara, N. Yamamoto, and S. Mori, Phys. Rev. Lett. **103**(20), 207601 (2009).
[29]H. Yan, F. Inam, G. Viola, H. Ning, H. Zhang, Q. Jiang, T. Zeng, Z. Gao, and M. J. Reece, J. Adv. Dielectr. **01**(01), 107 (2012).
[30]L. Wen, J. Yin, X. Wu, X. Wei, W. Liu, D. Yang, and J. Wu, Acta Mater. **255**, 119090 (2023).
[31]J. Li, X. Su, H.-H. Wu, J. Li, S. Qin, R. Yin, C. Liu, D. Guo, Y. Su, L. Qiao, T. Lookman, and Y. Bai, Scr. Mater. **216**, 114763 (2022).
[32]Z. Wu, W. Hu, K. Banerjee, H. Yan, and M. Zhang, Appl. Phys. Lett. **126**(23), 232903 (2025).
[33]A. Torelló and E. Defay, Adv. Electron. Mater. **8**(6), 2101031 (2022).
[34]F. Li, X. Ji, X. Wang, C. Dai, X. Wang, S. Chen, W. Liu, M. Long, L. Shan, H. Qi, J. Wang, C. Wang, and Z. Cheng, Adv. Funct. Mater. **35**(16), 2418534 (2024).
[35]R. Yin, J. Li, X. Su, S. Qin, C. Yu, Y. Hou, C. Liu, Y. Su, L. Qiao, T. Lookman, and Y. Bai, Adv. Funct. Mater. **32**(5), 2108182 (2021).
[36]W. L. Hsu, C. W. Tsai, A. C. Yeh, and J. W. Yeh, Nat. Rev. Chem. **8**(6), 471 (2024).
[37]L. Zhao, X. Ke, Z. Zhou, X. Liao, J. Li, Y. Wang, M. Wu, T. Li, Y. Bai, and X. Ren, J. Mater. Chem. C **7**(5), 1353 (2019).
[38]J. Li, D. Zhang, S. Qin, T. Li, M. Wu, D. Wang, Y. Bai, and X. Lou, Acta Mater. **115**, 58 (2016).
[39]F. Li, G. Chen, X. Liu, J. Zhai, B. Shen, S. Li, P. Li, K. Yang, H. Zeng, and H. Yan, Appl. Phys. Lett. **110**(18), 182904 (2017).
[40]J. Wu, H. Liu, H. Qi, B. Gao, L. Chen, W. Li, S. Deng, and J. Chen, J. Mater. Chem. A **10**(35), 18070 (2022).
[41]J. Koruza, B. Rožič, G. Cordoyiannis, B. Malič, and Z. Kutnjak, Appl. Phys. Lett. **106**(20), 202905 (2015).